International Journal of Information, Control and Computer Sciences
ISSN: 2517-9942
Vol:12, No:11, 2018

Multiscale Modelization of Multilayered Bi-Dimensional Soils

I. Hosni, L. Bennaceur Farah, N. Saber, R Bennaceur

***Abstract*—**Soil moisture content is a key variable in many environmental sciences. Even though it represents a small proportion of the liquid freshwater on Earth, it modulates interactions between the land surface and the atmosphere, thereby influencing climate and weather. Accurate modeling of the above processes depends on the ability to provide a proper spatial characterization of soil moisture. The measurement of soil moisture content allows assessment of soil water resources in the field of hydrology and agronomy. The second parameter in interaction with the radar signal is the geometric structure of the soil. Most traditional electromagnetic models consider natural surfaces as single scale zero mean stationary Gaussian random processes. Roughness behavior is characterized by statistical parameters like the Root Mean Square (RMS) height and the correlation length. Then, the main problem is that the agreement between experimental measurements and theoretical values is usually poor due to the large variability of the correlation function, and as a consequence, backscattering models have often failed to predict correctly backscattering. In this study, surfaces are considered as band-limited fractal random processes corresponding to a superposition of a finite number of one-dimensional Gaussian process each one having a spatial scale. Multiscale roughness is characterized by two parameters, the first one is proportional to the RMS height, and the other one is related to the fractal dimension. Soil moisture is related to the complex dielectric constant. This multiscale description has been adapted to two-dimensional profiles using the bi-dimensional wavelet transform and the Mallat algorithm to describe more correctly natural surfaces. We characterize the soil surfaces and sub-surfaces by a three layers geo-electrical model. The upper layer is described by its dielectric constant, thickness, a multiscale bi-dimensional surface roughness model by using the wavelet transform and the Mallat algorithm, and volume scattering parameters. The lower layer is divided into three fictive layers separated by an assumed plane interface. These three layers were modeled by an effective medium characterized by an apparent effective dielectric constant taking into account the presence of air pockets in the soil. We have adopted the 2D multiscale three layers small perturbations model including, firstly air pockets in the soil sub-structure, and then a vegetable canopy in the soil surface structure, that is to simulate the radar backscattering. A sensitivity analysis of backscattering coefficient dependence on multiscale roughness and new soil moisture has been performed. Later, we proposed to change the dielectric constant of the multilayer medium because it takes into account the different moisture values of each layer in the soil. A sensitivity analysis of the backscattering coefficient, including the air pockets in the volume structure with respect to the multiscale roughness parameters and the apparent dielectric constant, was carried out. Finally, we proposed to study the behavior of the backscattering coefficient of the radar on a soil having a vegetable layer in its surface structure.

I. Hosni, L. Bennaceur Farah and N. Saber are with LTSIRS, ENIT, Tunisia (e-mail: hosni_ibtissem@yahoo.fr; lilia.bennaceur@ipeit.rnu.tn; naceurs@yahoo.fr).

R. Bennaceur was with LMPC, FST, Tunisia (e-mail: raoufbennaceur@gmail.com).

***Keywords*—**Multiscale, bi-dimensional, wavelets, SPM, backscattering, multilayer, air pockets, vegetable.

I. Multiscale Modelization of Soil Roughness

THEwavelets weights (called wavelet coefficients) are the wavelet transform, which is therefore a function of two variables: time and scale (or dilation). In electromagnetic scattering modelization of rough soil, theoretical models (SPM IEM [1]) and empirical models [2] generally describe the surface using the autocorrelation function. Several studies have proved that backscattering coefficient σ is closely related to the form of this function [3], [4]. Thus, the choice of the analytical autocorrelation function (Gaussian or exponential) and its form used to adjust the experimental function is of paramount importance for proper simulation of radar signal.

A. Autocorrelation Function (ACF)

New approaches based on fractal analysis of the soil surface have improved the simulation of the radar signal with the integration of new roughness parameter which is the fractal dimension [5]:

$$\rho(x) = e^{-\left(\frac{x}{L}\right)} \text{exponential}$$

$$\rho(x) = e^{-\left(\frac{x}{L}\right)^2} \quad \text{gaussian}$$

$$\rho(x) = e^{-\left(\frac{x}{L}\right)^\tau} \quad \text{fractal}$$

with $\tau = -1.67D + 3.67, D$ is the fractal dimension calculated from the empirical correlation function that best fits the experimental function so that it lies between the Gaussian function and the exponential function.

B. Autocorrelation Function (ACF)

The natural rough surfaces have different structures in all directions, especially in two perpendicular directions. In this case, the one-dimensional description is inadequate, anda two-dimensional processing is required.

In the 2D case, the two-dimensional scale function $\varphi\,(x, y)$ and the 2D three wavelets, $\psi h, \psi v, \psi d$ are defined as follows:

$$\phi(x, y) = \varphi\,(x)\varphi(y) \tag{1}$$

$$\psi^h(x, y) = \varphi\,(x)\psi(y) \tag{2}$$

$$\psi^v(x, y) = \psi\,(x)\varphi(y) \tag{3}$$

$$\psi^d(x, y) = \psi\,(x)\psi\,(y) \tag{4}$$

Thus, in the present case, the modeled surface is considered as a collection of elementary surfaces of size B (external spatial scales number). The horizontal, vertical, and diagonal components produced by the decomposition of z (x, y) into wavelets are given by:

Horizontal component:

$$z_P^H(x,y) = \sum_{m_x=0}^{P}\sum_{m_y=0}^{P}\sum_{n_x=-\infty}^{+\infty}\sum_{n_y=-\infty}^{+\infty} z_{n_x}^{m_x} z_{n_y}^{m_y}\, \psi\left(\frac{2^{m_x}}{B}x - n_x\right)\phi\left(\frac{2^{m_y}}{B}y - n_y\right) \quad (5)$$

Vertical component:

$$z_P^V(x,y) = \sum_{m_x=0}^{P}\sum_{m_y=0}^{P}\sum_{n_x=-\infty}^{+\infty}\sum_{n_y=-\infty}^{+\infty} z_{n_x}^{m_x} z_{n_y}^{m_y}\, \phi\left(\frac{2^{m_x}}{B}x - n_x\right)\psi\left(\frac{2^{m_y}}{B}y - \mathrm{n_y}\right) \quad (6)$$

Diagonal component:

$$z_P^D(x,y) = \sum_{m_x=0}^{P}\sum_{m_y=0}^{P}\sum_{n_x=-\infty}^{+\infty}\sum_{n_y=-\infty}^{+\infty} z_{n_x}^{m_x} z_{n_y}^{m_y}\, \psi\left(\frac{2^{m_x}}{B}x - n_x\right)\psi\left(\frac{2^{m_y}}{B}y - \mathrm{n_y}\right) \quad (7)$$

where the scale function is given by: $\phi_{n_i}^{m_i} = \phi\left(\frac{2^{m_i} i}{B} - n_i\right)$, and $\psi_{n_i}^{m_i} = \psi\left(\frac{2^{m_i} i}{B} - n_i\right)$ is the mother wavelet, $i = x \text{or } y$.

The autocorrelation functions (ACF) associated with the horizontal, vertical and diagonal components are expressed as follows:

Horizontal component:

$$\rho^H(x,y,x+\xi,y+\eta) = \langle z_P^H(x,y) z_P^H(x+\xi,y+\eta)\rangle \quad (8)$$

Vertical component:

$$\rho^V(x,y,x+\xi,y+\eta) = \langle z_P^V(x,y) z_P^V(x+\xi,y+\eta)\rangle \quad (9)$$

Diagonal component:

$$\rho^D(x,y,x+\xi,y+\eta) = \langle z_P^D(x,y) z_P^D(x+\xi,y+\eta)\rangle \quad (10)$$

In Figs. 1-9, the two perpendicular axes present respectively the spatial extension in x (cm) and the spatial extension in y (cm).

Figs. 1-3 show the variations of the three autocorrelation function components for two-dimensional surfaces characterized by the same multiscale parameters of soil roughness: $\nu x = 1.1$; $\nu y = 1.1, \gamma x = 0.2\, cm$ and $\gamma y = 0.2\, cm$.

We can notice that the vertical and horizontal components have similar aspect in perpendicular directions.

In Figs. 4-9, we studied the effect of P (spatial scales number) on the autocorrelation function form by representing the three components of ACF of the same surfaces (with $P = 7$ and $P = 13$).

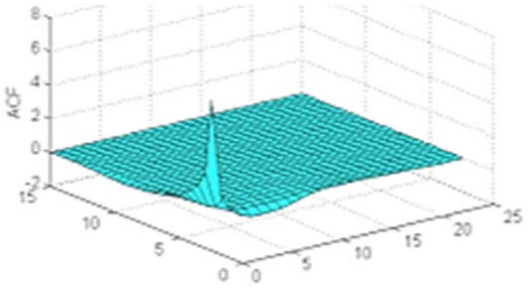

Fig. 1 ACF horizontal component: $\boldsymbol{\nu x = 1.1}$; $\boldsymbol{\nu y = 1.1}$; $\boldsymbol{\gamma x = 0.2\ cm}$; $\boldsymbol{\gamma y = 0.2\ cm}$

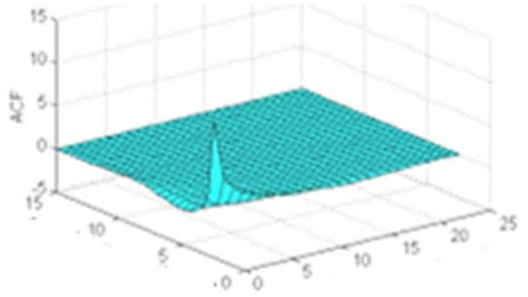

Fig. 2 ACF vertical component: $\nu x = 1.1$; $\nu y = 1.1$; $\gamma x = 0.2$ cm; $\gamma y = 0.2$ cm

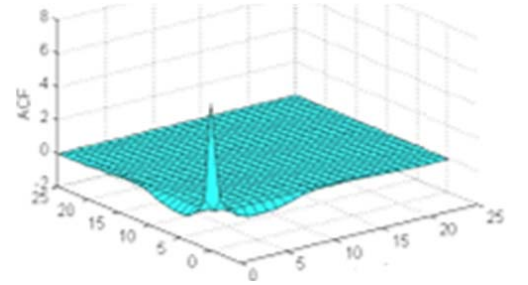

Fig. 3 ACF diagonal component: $\nu x = 1{,}1$; $\nu y = 1{,}1$; $\gamma x = 0{,}2$cm; $\gamma y = 0{,}2$ cm

- *Horizontal Component*

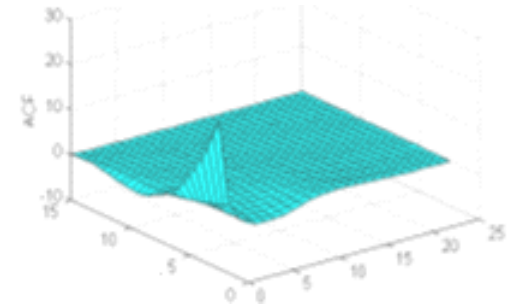

Fig. 4 ACF horizontal component: $\boldsymbol{\nu x = 2.1}$; $\boldsymbol{\nu y = 1.1}$; $\boldsymbol{\gamma x = 0.2\ cm}$; $\boldsymbol{\gamma y = 0.8\ cm}$ **and** $\boldsymbol{P = 7}$

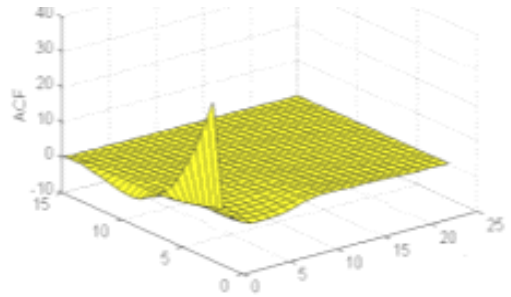

Fig. 5 ACF horizontal component: $vx = 2.1$; $vy = 1.1$; $\gamma x = 0.2\ cm$; $\gamma y = 0.8\ cm$ *and* $P = 13$

- *Vertical Component*

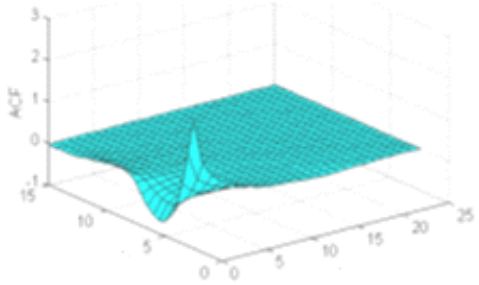

Fig. 6 ACF vertical component: $\mathbf{vx = 2.1}$; $\mathbf{vy = 1.1}$; $\boldsymbol{\gamma x} = \mathbf{0.2\ cm}$; $\boldsymbol{\gamma y} = \mathbf{0.8\ cm}$ **and** $\mathbf{P = 7}$

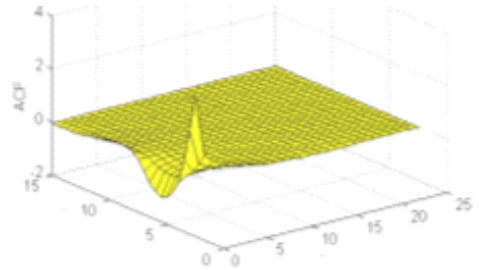

Fig. 7 ACF vertical component: $vx = 2.1$; $vy = 1.1$; $\gamma x = 0.2\ cm$; $\gamma y = 0.8\ cm$ *and* $P = 13$

- *Diagonal component*

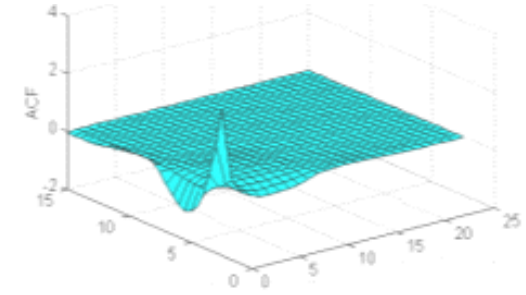

Fig. 8 ACF diagonal component: *vx= 2.1; vy = 1.1; yx= 0.2 cm; yy = 0.8 cm and Zmax = 3.7 cm* $\mathbf{vx = 2.1}$; $\mathbf{vy = 1.1}$; $\boldsymbol{\gamma x} = \mathbf{0.2\ cm}$; $\boldsymbol{\gamma y} = \mathbf{0.8\ cm}$ **and** $\mathbf{P = 7}$

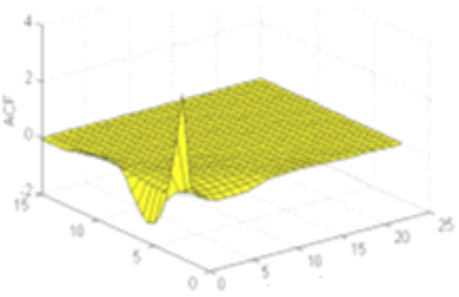

Fig. 9 ACF diagonal component: $vx = 2.1$; $vy = 1.1$; $\gamma x = 0.2\ cm$; $\gamma y = 0.8\ cm$ *and* $P = 13$

C. Wavelet Type Effect in the Calculation of the ACF

Figs. 10-13 show shapes of the autocorrelation function for different types of wavelets.

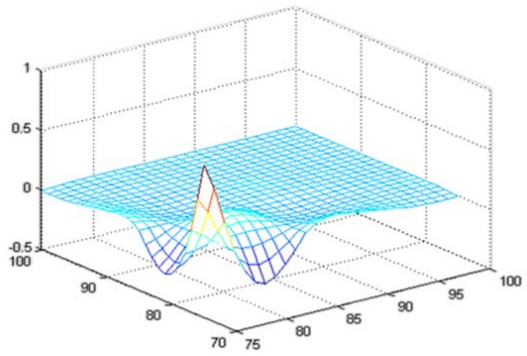

Fig. 10 Multiscale ACF with Daubechies4 wavelet

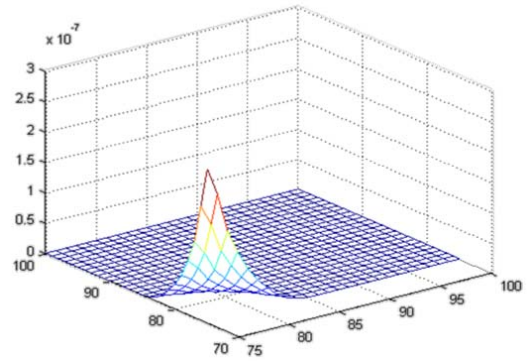

Fig. 11 Multiscale ACF with Hamar wavelet

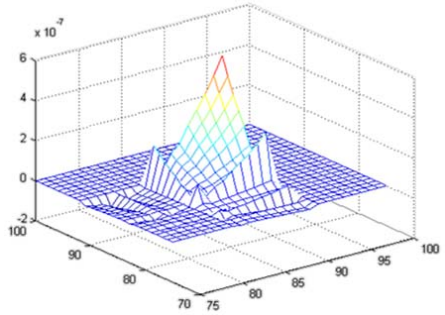

Fig. 12 Multiscale ACF with Meyer wavelet

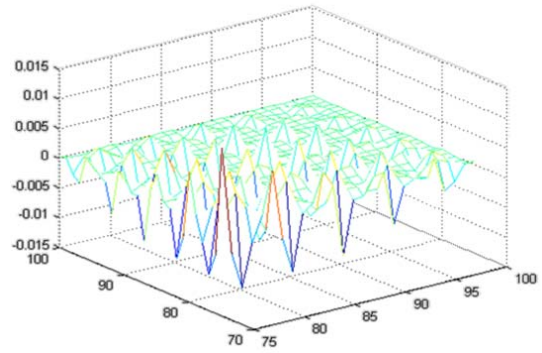

Fig. 13 Multiscale ACF with Morlet wavelet

The wavelets used in this work are Daubechiesfour wavelets. The number 4 in this wavelet type explains that this transformation has four coefficients of wavelet and scaling functions.

D. Representations of 3D Multi-Scale Surfaces

The following figures correspond to the three-dimensional representations of the multi-scale surfaces for different values of roughness parameters. We have studied the effects of the variation of multi-scale parameters, namely ν (parameter related to the fractal dimension) and P (the number of spatial scales). In Figs. 14 and 15, the parameter ν linked to multi-scale fractal structure has been varied.

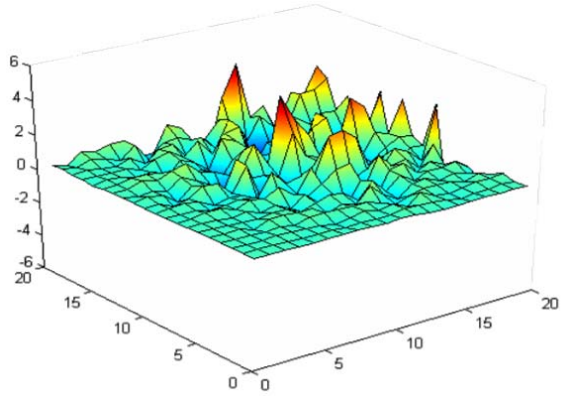

Fig. 14 3D representation of the height of a multiscale two-dimensional surface: *vx= vy = 1.1; yx= y1 =0.2 cm; γy = γ2 = 0.3 cm, Zmax = 3.7 cm*

It can be noted that for $\nu = 1.1$, the surface is rougher with a maximum of 3.7 cm, whereas for $\nu = 2.1$ it is smoother with a maximum of 2.3 cm.In Figs. 16 and 17, the 3D structure of a multi-scale surface is represented for two different numbers of spatial scales, P = 5 and P = 7 with the same roughness parameters. We observed that by increasing P, the structure of the surface is more complex and more varied.

In the following section, we will study the modelization of backscattering signal by using the multi-scale description of rough surfaces and we will focus on the sensitivity of the modelized radar signal with respect to the different parameters on which it depends, intrinsic (as frequency, polarization, incidence angle) and extrinsic (multiscale roughness and moisture).

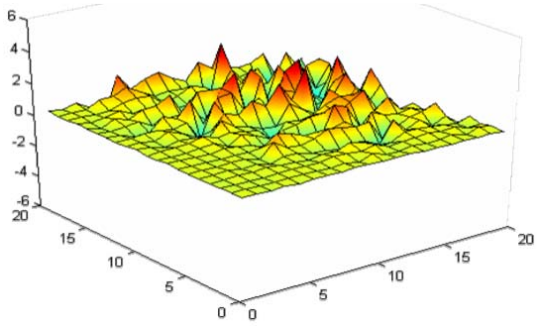

Fig. 15 3D representation of the height of a multiscale two-dimensional surface: *vx= vy = 2.1; yx= y1 =0.2 cm; γy = γ2 = 0.3 cm, Zmax = 2.3 cm*

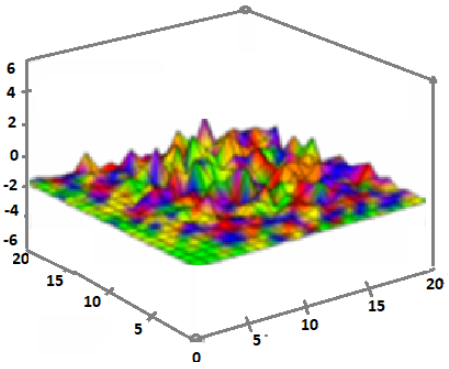

Fig. 16 3D representation of the height of a multiscale two-dimensional surface: *vx = vy = 1.3; γy = γx = 0.3 cm; P = 5*

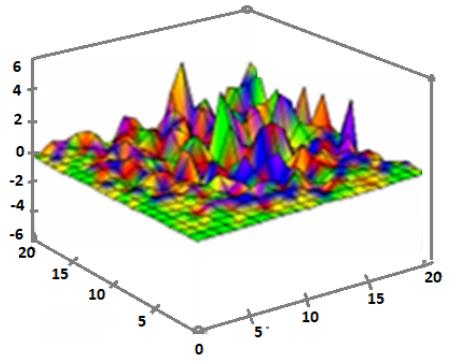

Fig. 17 3D representation of the height of a multiscale two-dimensional surface: $vx = vy = 1.3$; $\gamma y = \gamma x = 0.3\,cm$; $P = 7$

II. Three-Layered Multi-Scale SPM Model

This section is about studding the impact of the multi-scale three-layered description on the radar backscattering coefficient by using the SPM model adapted to three-layered multi-scale surfaces with low roughness, using parameters values in correspondent validity domain.

A. Proposed Description of the Studied Soil

In order to analyze the effects of the dielectric permittivity profile, we have introduced a modification of the Fresnel coefficients of the SPM model by integrating the criterion of three fictitious layers $(0-1\ cm, 1-2\ cm, 2-5\ cm)$ (Fig. 18).

A multilayered approach for reflection phenomenon has been conceptually chosen because actually there is no real physical layer, but rather a continuous variability. We proposed to use a surface diffusion model with surface permittivity. We introduced thereafter the hypothesis of the layers and we calculated an effective permittivity. It includes the different dielectric permittivities of the three fictitious layers, and a new estimated Fresnel reflection coefficient is carried out.

Fig. 18 shows a conceptual representation of the soil surface in the first five centimeters. This surface consists of three layers separated by an interface supposed to be plane. Each layer has its own characteristics: a relative permittivity ε_r, a thickness d and a reflection coefficient R.

At this stage, and in order to be able to calculate the new effective permittivity, we must foremost modify the expression of Fresnel reflection coefficients of the SPM model. These coefficients control the reflection phenomenon of electromagnetic waves at the interface between two media, having two different refractive indices. They indicate the links existing between the amplitudes of the reflected and transmitted waves and the amplitude of the incident wave.

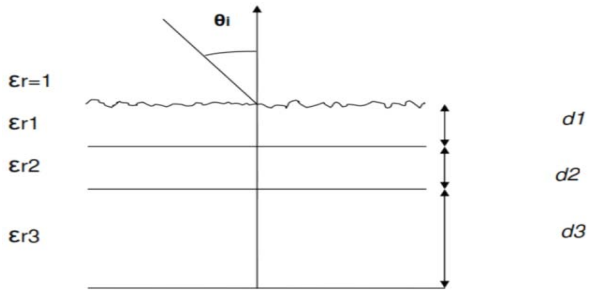

Fig. 18 Conceptual representation of the surface

B. Modification of the Fresnel Reflection Coefficients

Actually, there are no physical boundaries between the different layers, and therefore the soil is characterized by a continuous dielectric profile. The hypothesis of the existence of three distinct layers in the soil is a result of an incoherent treatment caused by the interference of multiple reflections.

According to the Fung article [6], the reflection coefficient is expressed as follows:

$$R_{2i} = \frac{R_0 + R_1 * \exp(-2\alpha d)}{1 + R_0 + R_1 * \exp(-2\alpha d)} \quad (11)$$

with R_1 et R_2 are the Fresnel reflection coefficients at the layer boundaries, R_0 is the Fresnel reflection coefficient of the added layer, d defines the thickness of the layer, and α is the parameter on which depends the relative dielectric permittivity ε_r and the wavelength of the layer in vacuum wave λ_0.

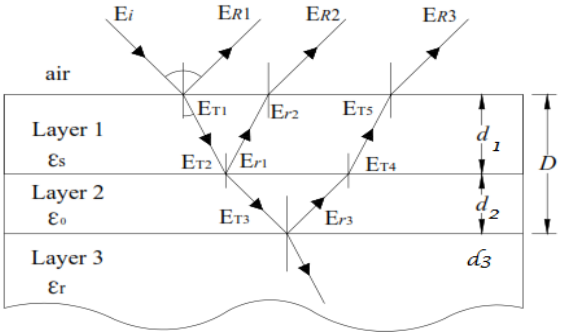

Fig. 19 Representation of multi -layered model and existing phenomena of reflection / refraction between layers

The corresponding effective permittivity is presented by the following equation:

$$\varepsilon_{eff}(z) = \left(\frac{1+R_{2i}}{1-R_{2i}}\right)^2 \quad (12)$$

For the proposed soil description, the coefficients R_0, R_1, R_2 present the Fresnel reflection coefficients at the boundaries of the three distinct layers of the soil. The indices h and v denote respectively the two orthogonal polarizations (horizontal and vertical). The Fresnel reflection coefficient air/layer1 is defined by:

$$R_0^h = \frac{cos\theta_i - \sqrt{\varepsilon_{r1} - sin^2\theta_i}}{cos\theta_i + \sqrt{\varepsilon_{r1} - sin^2\theta_i}} \quad (13)$$

$$R_0^v = \frac{\varepsilon_1 cos\theta_i - \sqrt{\varepsilon_1 - sin^2\theta_i}}{\varepsilon_1 cos\theta_i - \sqrt{\varepsilon_1 - sin^2\theta_i}} \quad (14)$$

The Fresnel reflection coefficient first-layer/second-layer is defined by:

$$R_1^h = \frac{cos\theta_i - \sqrt{\varepsilon_{r2}/\varepsilon_{r1} - sin^2\theta_i}}{cos\theta_i + \sqrt{\varepsilon_{r2}/\varepsilon_{r1} - sin^2\theta_i}} \quad (15)$$

$$R_1^v = \frac{\varepsilon_2\sqrt{\varepsilon_1 - sin^2\theta_i} - \varepsilon_1\sqrt{\varepsilon_2 - sin^2\theta_1}}{\varepsilon_2\sqrt{\varepsilon_1 - sin^2\theta_i} + \varepsilon_1\sqrt{\varepsilon_2 - sin^2\theta_1}} \quad (16)$$

The Fresnel reflection coefficient second-layer/third-layer is defined by:

$$R_2^h = \frac{cos\theta_i - \sqrt{\varepsilon_{r3}/\varepsilon_{r2} - sin^2\theta_i}}{cos\theta_i + \sqrt{\varepsilon_{r3}/\varepsilon_{r2} - sin^2\theta_i}} \quad (17)$$

$$R_2^v = \frac{\varepsilon_3\sqrt{\varepsilon_2 - sin^2\theta_1} - \varepsilon_2\sqrt{\varepsilon_3 - sin^2\theta_2}}{\varepsilon_3\sqrt{\varepsilon_2 - sin^2\theta_1} + \varepsilon_2\sqrt{\varepsilon_3 - sin^2\theta_2}} \quad (18)$$

The coefficients of the considered three layers are in the following form:

$$R_{2-5cm} = R_2 \quad (19)$$

$$R_{1-2cm} = \frac{R_1 + R_2 * exp\left[-2*\left(\frac{2*\pi}{\lambda_0} * ima(\sqrt{\varepsilon_{r2}})\right)*d_2\right]}{1 + R_1 R_2 * exp\left[-2*\left(\frac{2*\pi}{\lambda_0} * ima(\sqrt{\varepsilon_{r2}})\right)*d_2\right]} \quad (20)$$

The reflection model based on a multilayer approach consists of three fictitious layers. We have taken into account assumptions to respect:

- The mixture of soil particles and liquid water is horizontally and vertically uniform, thereby the distribution of complex and constant dielectric variables is as well uniform.
- Multiple refractions between different interfaces in the reflection model are ignored, thus only the reflection of the upper interface is considered.

The incidence and reflection angles of the radar signal can be written as follows:

$$E_i = E_0 exp^{-jk_{1z}z} \quad (21)$$

$$E_{R1} = R_a E_0 exp^{-jk_{1z}z} \quad (22)$$

$$E_{R2} = T_{10} A R_s A T_{01} E_i \quad (23)$$

$$E_{R3} = T_{10} A T_{21} R_a T_{12} A T_{01} E_i \quad (24)$$

where $k_{1z} = k_1 cos\theta$, θ and k_1 are respectively the incidence angle and the waves. Number. $E_0$and$exp^{-jk_{1z}z}$ are respectively the incident waves amplitude and phase, $R_a$is the air specular reflection coefficient, $R_s$is the reflection coefficient of the interface, $T_{mn}$is the transmission coefficient from layer m to layer n, A is the amplitude of the attenuation factor given by the following formula:

$$A = exp^{-K_e d_1 / cos\theta_t} \quad (25)$$

where$K_e$is the extinction coefficient of the first layer, d_1 is its thickness, θ_t is the reflection angle of the first layer interface in the case. Based on the preceding equations, we can calculate the total reflection coefficient of the soil multilayer reflection model, given by the following equation:

$$\tilde{R}_a = R_a + R_a T_{01} T_{10} A^2 (T_{01} T_{10} + 1) \quad (26)$$

with:

$$T_{01} = 1 + R_{01} = 1 + R_a \quad (27)$$

$$T_{10} = 1 + R_{10} = 1 - R_a \quad (28)$$

This model includes two variables:

- Specular reflection variable R_a, it corresponds to the energy amount of the dispersed radar signal by the natural soil surface;
- Volume dispersion variable:$T_{01} T_{10} A^2 (R_{as} T_{01} T_{10} + R_a)$, it describes the internal reflections between layers.

In these multilayer reflections model, the thickness of the first layer d_1 is a key parameter. If we assume that the propagation of the radar signal is from one layer to another and assume that the radar penetration depth is D, then we obtain:

$$D = d_1 + d_2 + d_3 \quad (29)$$

Since the total volume of the natural soil is the sum of the voids, the mixture of soil particles and the liquid water, we have:

$$d_1 = D(1 - \phi) \quad (30)$$

whereϕ defines the percentage of voids volume in the total soil volume.

C. Sensitive Analysis of the Three-Layered Multi-Scale SPM Backscattering Model

1) Presentation of the New Parameters

The measurement of soil moisture, closely related to the dielectric constant ε [7], [8], allows the evaluation of soil water resources in the field of water, hydrology and agronomy [9]. The second soil parameter interacting with the radar signal is the geometric structure.

In this context, many previous works in the mathematical description of surfaces in different application domains and spatial scales [10], [11] often concluded that natural surfaces are better characterized by a stationary random process [12]. The distribution of heights defining the roughness of the soil is considered as a superposition of a finite number of one-dimensional fractal Gaussian processes, having each one a different spatial scale [13], [14]. This multi-scale roughness is represented by two new multi-scale parameters;ν and γ related respectively to the fractal dimension D and the standard deviation of the heights s [12].

The SPM Model has been modified, using a two-dimensional multi-resolution description of three-layered soils, in order tomodelise the radar response and to simulate radar backscattering coefficients. The input parameters of this model are:

- The dielectric constant (derived from the volume water content of the surface), the parameter ν related to the fractal dimension and the γ parameter related to the standard deviation of the heights.

The backscattering coefficients of the three-layered surface, for both vertical and parallel polarizations can be expressed as follow:

$$\sigma_{vv} = 8k^4\sigma_1^2 \left| R_{\parallel} cos^2\theta + \frac{sin^2\theta(1+R_{\parallel})^2}{2}\left(1 - \frac{1}{\varepsilon_r}\right)\right|^2 W(2ksin\theta, 0) \quad (31)$$

$$\sigma_{hh} = 8k^4\sigma_1^2 |R_{\perp} cos^2\theta|^2 W(2ksin\theta, 0) \quad (32)$$

$$W^n(-2k_x, 0) = \frac{2}{\pi}\int_0^{\infty}\int_0^{\infty}\left(\frac{r_c^i(\xi,\eta)}{r_c^i(0,0)}\right)^n \cos(2k_x\xi)d\xi d\eta \quad (33)$$

$\theta$is the incident angle, the expression of I_{qp} is given by Fung [6]. $W^n$is the nth Fourier transform of the autocorrelation function given by Mattia, with n = 1 for the SPM model [12]-[15], [16].

2) The Effect of Multi-Scale Roughness on the Backscattering Coefficient

Figs. 20-31, 35-38, and 42-49 present the backscattering coefficient (dB) as a function of the incident angle (degrees).

At first, the value of γ was set at $0.0031m$ (Figs. 20 and 21), the parameter related to the fractal dimension ν was varied from 1.3 to 2.1 for the two polarizations HH and VV with five spatial scales.

It can be noted that the backscattering coefficient σ decreases as the increasing of the incident angle θ. Otherwise, as the parameter ν increases, the backscattering coefficient decreases. This can be explained by the fact that the surfaces become smoother and the diffusion properties are dominated by specular reflection.

In a second step, the value of ν was set at 1.3 and γ was varied from $0.0011\ m$ to $0.0051\ m$ (Figs. 22 and 23).

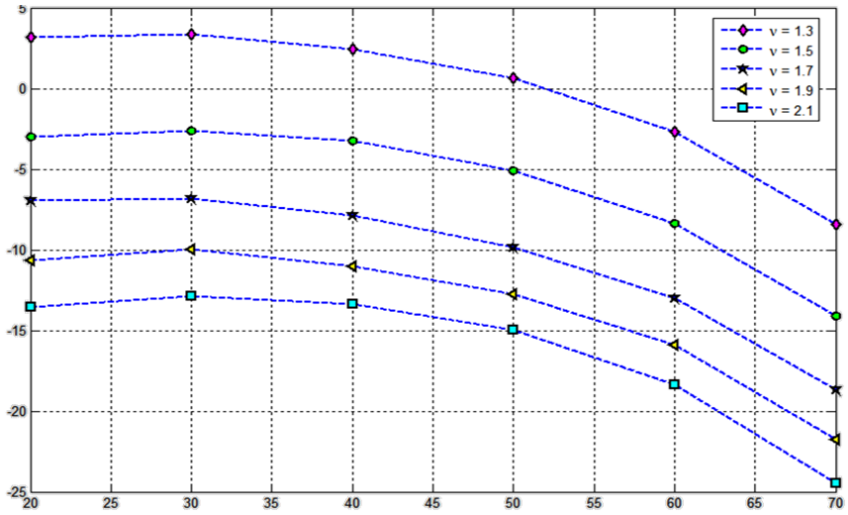

Fig. 20 σ_{HH} as a function of the incident angle θ for different values of ν

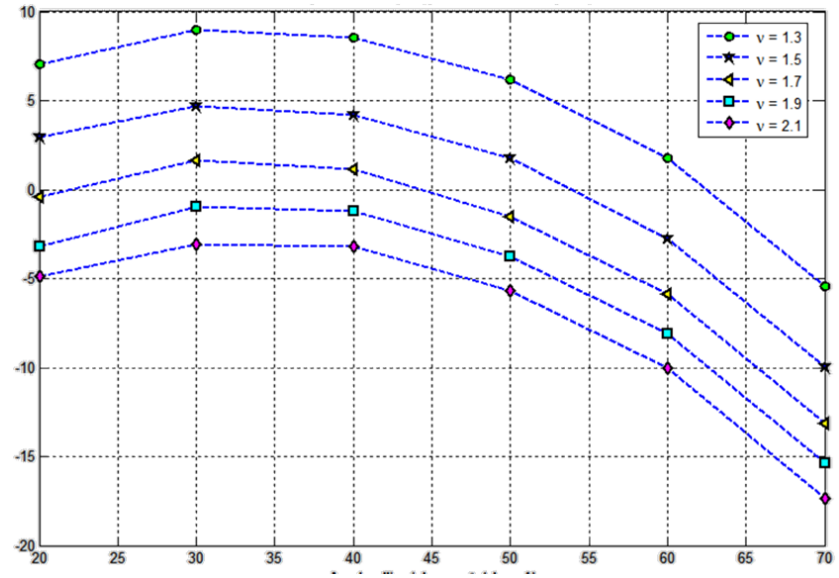

Fig. 21 σ_{VV} as a function of the incident angle θ for different values of ν

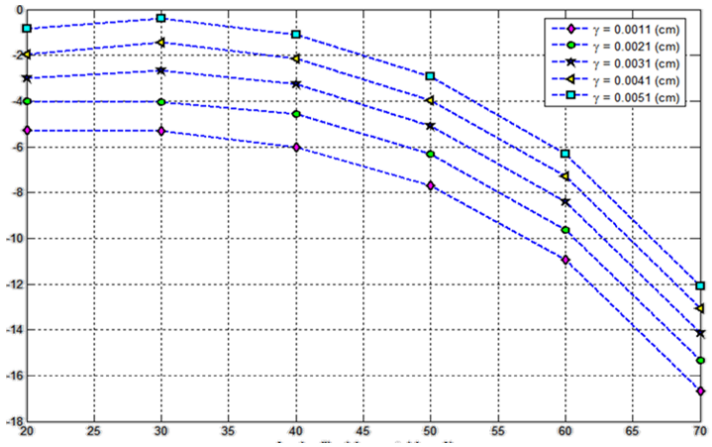

Fig. 22 σ_{HH} as a function of the incident angle θ for different values of γ

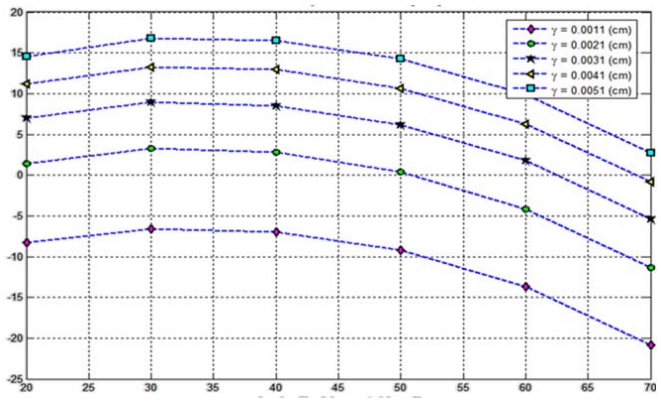

Fig. 23 $\boldsymbol{\sigma_{VV}}$ as a function of the incident angle $\boldsymbol{\theta}$ for different values of $\boldsymbol{\gamma}$

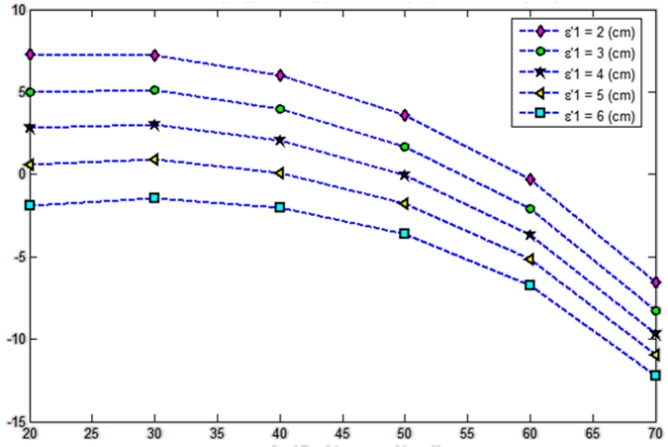

Fig. 24 σ_{HH} as a function of the incident angle θ for different values of ε_1

In both cases, we see that the backscattering coefficient increases with the increasing of γ.

3) The Effect of Moisture on the Backscattering Coefficient

The humidity is related to the complex dielectric constant, ε_1 and ε_2 denote the real and the imaginary part of the dielectric constant ε.

At first, we studied the impact of ε_1 on radar signal backscattering by setting ε_2 at 10 (Figs. 24 and 25) and varying ε_1 from 2 to 6, respectively for both HH and VV polarizations. We can note that the backscattering coefficient

decreases when the complex dielectric constant ε_1 increases.

In Figs. 26 and 27, ε_1 was set at 5. For VV polarization, we varied ε_2 from 8 to 12 and from 6 to 10 for the HH polarization.

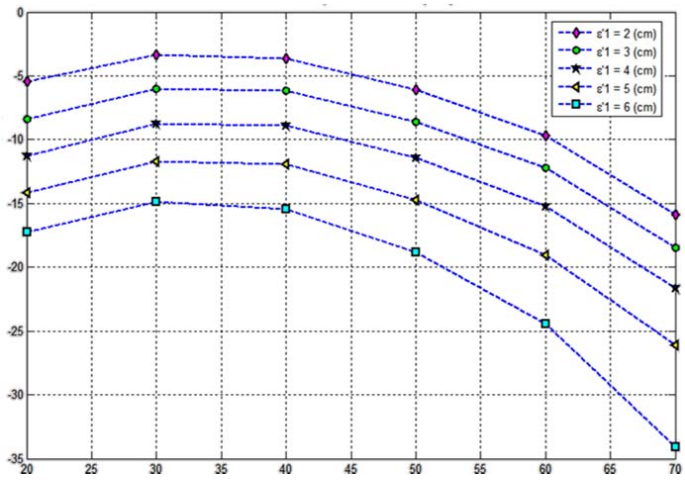

Fig. 25 σ_{VV} as a function of the incident angle θ for different values of ε_1

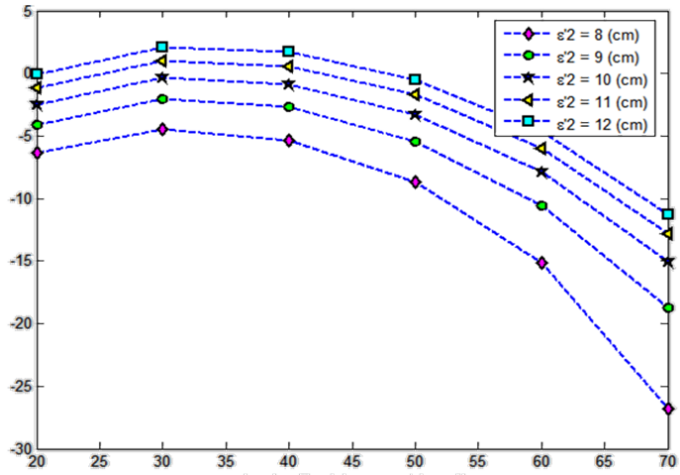

Fig. 26 $\boldsymbol{\sigma_{VV}}$ as a function of the incident angle $\boldsymbol{\theta}$ for different values of $\boldsymbol{\varepsilon_2}$

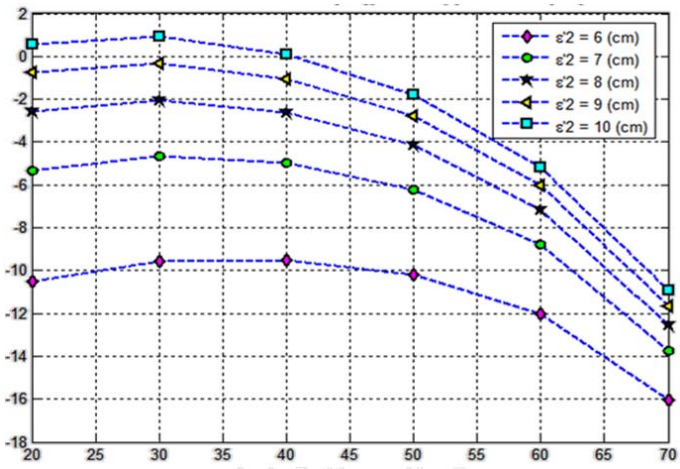

Fig. 27 σ_{HH} as a function of the incident angle θ for different values of ε_2

It can be noted that the backscattering coefficient increases as well ε_2 increases.

4) The Effect of Spatial Scales Number on the Backscattering Coefficient

We studied the effect of the number of spatial scales (Figs. 28 and 29) corresponding to an increase of the outer spatial scale on the backscattering coefficient for surfaces having the same multi-scale roughness parameters ν and γ in both HH and VV polarizations.

These backscattering plots clearly show that these surfaces have the same multiscale roughness characteristics but a different number of spatial scales, produce substantially different backscattering coefficients.

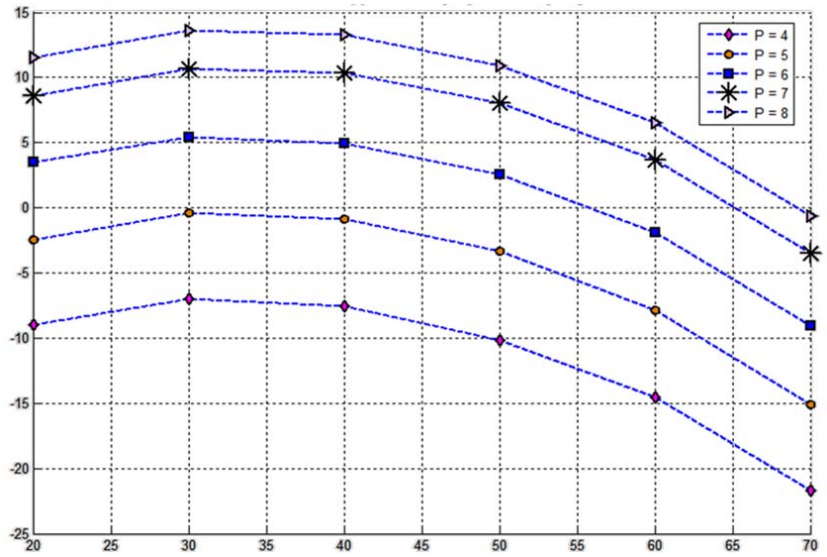

Fig. 28 σ_{VV} as a function of the incident angle θ for different values of P

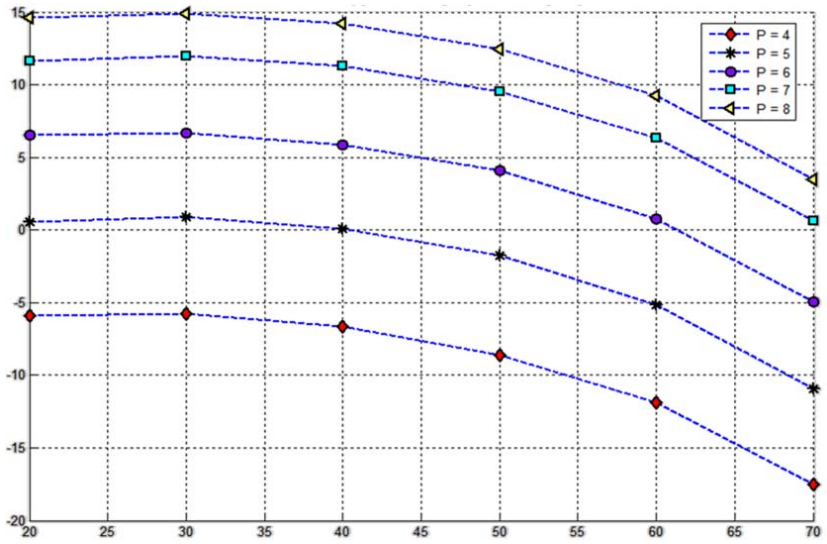

Fig. 29 $\boldsymbol{\sigma_{HH}}$ as a function of the incident angle $\boldsymbol{\theta}$ for different values of $\boldsymbol{P}$

Indeed, we see that when we go from 4 to 8 spatial scales, the backscattering coefficient rose by 19 dB. This could be explained by the fact that the surfaces having a large number of spatial scales, are more sensitive to the roughness variations resulting an increase of the specular scattering.

5) Incident Wave Frequency Effect on the Backscattering Coefficient

We studied the effect of the frequency of the incident wave on the backscattering for different values of roughness and humidity parameters. To this end, there is shown in Figs. 30 and 31 the variations of backscattering coefficient for five different frequencies ranging from 0.5 GHz to 0.9 GHz.

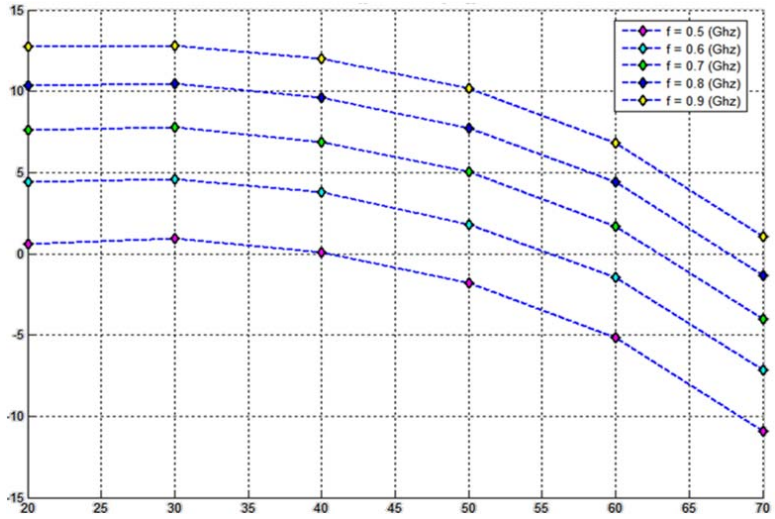

Fig. 30 $\boldsymbol{\sigma_{HH}}$ as a function of the incident angle $\boldsymbol{\theta}$ for different values of frequency $\boldsymbol{f}$ (GHz)

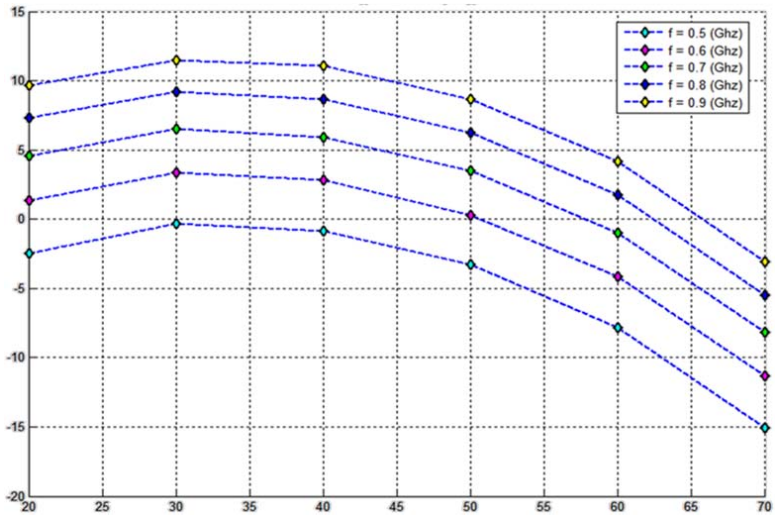

Fig. 31 σ_{VV} as a function of the incident angle θ for different values of frequency f (GHz)

We observed that the frequency variation effect induced a translation of the curve with signal amplification. This signal amplification can be explained by the fact that an increase in the frequency of the signal induced an increase in the imaginary part of the complex dielectric constant proportional inversely to the penetration depth and therefore an increase in moisture. Thus, higher the frequency, greater the backscattered signal strength and less the penetration depth.

III. Soil Subsurface Modelization

The air in the soil is vital for the respiration of roots and soil organisms, it also affects soil drainage, because more air pockets, greater the drainage is fast. Rough agricultural parcels have clods on their surfaces, including air fractions therebetween. We proposed to redefine the dielectric constant to include these air fractions presented in the volume of soil structure, taking into account the multiscale multilayer description of the soil.

A. Air Pockets Introduction in the Volume Structure of the Soil

Natural soilscontain air fractions. Previous works [13] modified the expression of the dielectric constant to take account of air pockets. The presence of air fractions is an influencing factor of the relationship between soil moisture and backscattering coefficient of the radar signal from a studied site to another and from a plot to another. The roughness description does not solve the problem gap between measurement and simulation, account must be taken of the work on agricultural fields and natural phenomena such as erosion, rain, etc.

The aim is to study the impact of new multiscale descriptive parameters of the surface, namely the γ parameter related to the standard deviation of the heights and the ν related to the fractal dimension parameter on the radar backscattering while taking into account the impact of air pockets included in the subsoil, and the modification of the scattering SPM (MLS 2D

three-layered model) using the two-dimensional wavelet transform and Mallat multi resolution algorithm [17].

1) Reflection of a Multilayer Medium

We have considered the soil, as illustrated in Fig. 32, as a three-layered medium, where D is the penetration depth of the radar signal. The multilayer model of the soil has three uniform layers [14].

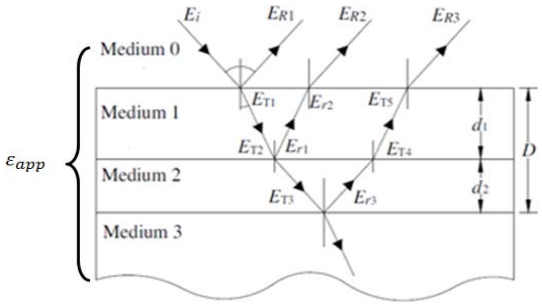

Fig. 32 Reflection multilayered model of the soil [14]

Medium 0 is a half-space. Medium 1, with d_1 as its thickness and ε_1 as its permittivity. Medium 2, which shows the air particles in the subsoil, with d_2 as its thickness and ε_2 as its permittivity. Medium 3 represents the undersoil layer below the penetration depth level of the radar signal D $(d_1 + d_2)$, with a permittivityε_3: it is a semi-infinite layer which has no thickness. E_i and E_r are respectively the incident and reflected radar signal [14]. We have introduced multilayer aspect of the surface soil humidity, and thereafter, the dielectric constant is designed to be redefined according to the new description to take into consideration the air/soil composition. $\varepsilon_{app}$is an effective permittivity that encompasses different dielectric permittivities of the three layers.

$$\varepsilon_{app} = [v_{sol} * \varepsilon_{sol}^{\alpha} + (1 - v_{sol}) * \varepsilon_{air}^{\alpha}]^{\frac{1}{\alpha}} \quad (34)$$

α = 0.5, ε_{sol} is the dielectric constant of the soil, ε_{air} is the dielectric constant of air, and $v_{sol}$is the fraction of the soil defined as:

$$v_{sol} = -0.22\, Log(Z_s) + 0.0058 \quad (35)$$

$$Z_s = s^2/l \quad (36)$$

The volumetric water content is given by m_v:

$$m_v = -5.3\ 10^{-2} + 2.92\ 10^{-2}\varepsilon_{app} - 5.5\ 10^{-4}{\varepsilon_{app}}^2 + 4.3\ 10^{-6}{\varepsilon_{app}}^3 \quad (37)$$

Figs. 33 and 34 show the impact of various variables, namely v_{sol} (the fraction of the soil) and m_v(soil moisture) on the volumetric water content of the soil.

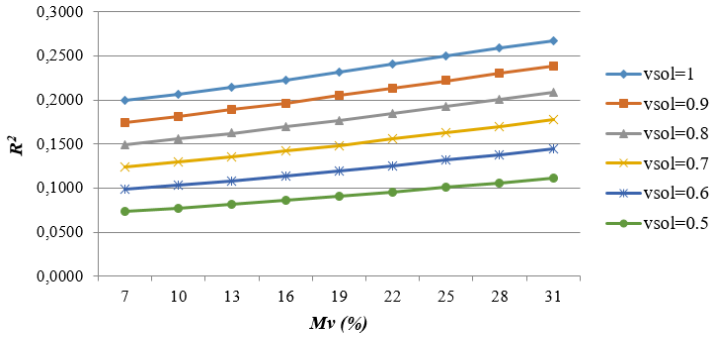

Fig. 33 $\boldsymbol{R^2}$ Variation as a function of moisture for different values of $\boldsymbol{v_{sol}}$ R^2 is the squared modulus of the Fresnel reflection coefficient

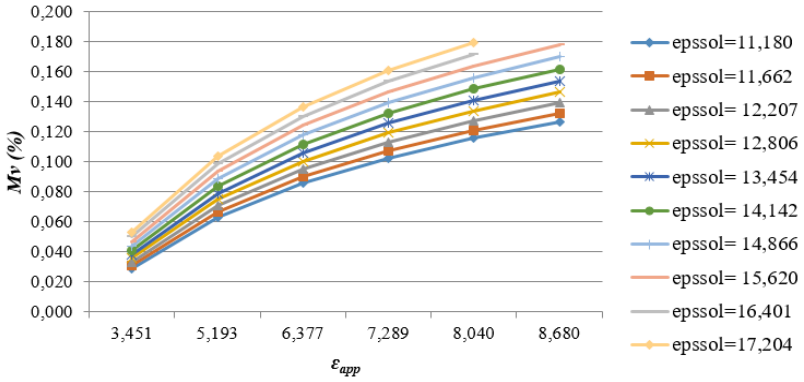

Fig. 34 $\boldsymbol{\varepsilon_{app}}$ impact on moisture for different values of $\boldsymbol{\varepsilon_{sol}}$

It may be noted that the volumetric soil moisture incremented simultaneously with the increase in the values of the parameters listed above.

2) Sensitive Analysis of Multiscale TrilayerSPM

We studied the backscattered radar signal sensitivity on a multiscale three-layered soil with different moisture and multiscale roughness values of each layer, and while taking account of the air pockets included in it.

- *The impact of multi-scale roughness parameters on the backscattering coefficient*

We set γ, the parameter related to the standard deviation of the heights, at 0.0031m with five spatial scales (Figs. 35 and 36).

It may be noted that when the fractal dimension increases, the surface becomes smoother, and the value of the backscattering coefficient down due to specular reflection. Then, we set ν, the parameter related to the fractal dimension, at 1.9 with P = 5, we varied the multiscale parameter related to the standard deviation of the heights γ (Figs. 37 and 38). The value of the backscattering coefficient increases, because an increase in the vertical roughness can cause amplification of the backscattered signal.

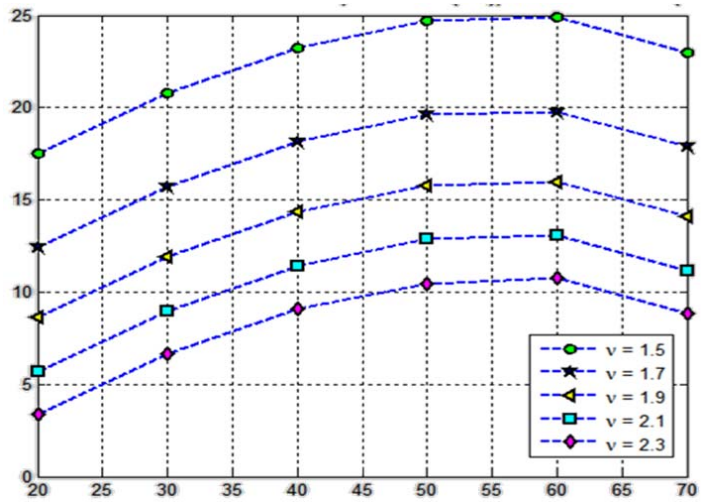

Fig. 35 $\boldsymbol{\sigma_{VV}}$ as a function of the incident angle $\boldsymbol{\theta}$ for different values of $\boldsymbol{\nu}$

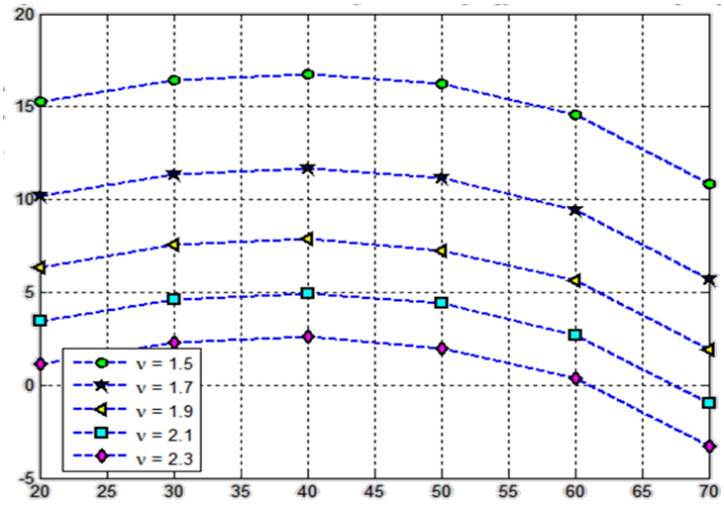

Fig. 36 $\boldsymbol{\sigma_{HH}}$ as a function of the incident angle $\boldsymbol{\theta}$ for different values of ν

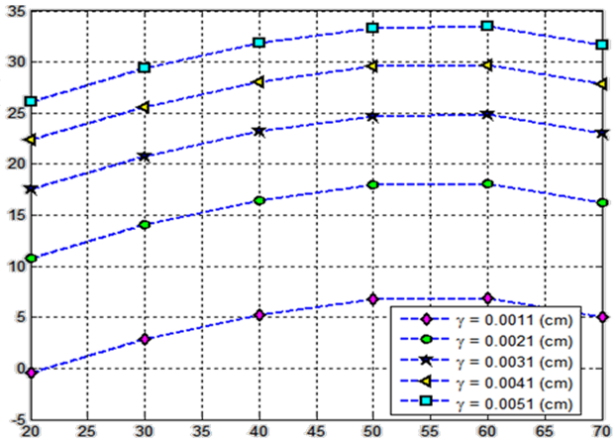

Fig. 37 $\boldsymbol{\sigma_{VV}}$ as a function of the incident angle θ for different values of $\boldsymbol{\gamma}$

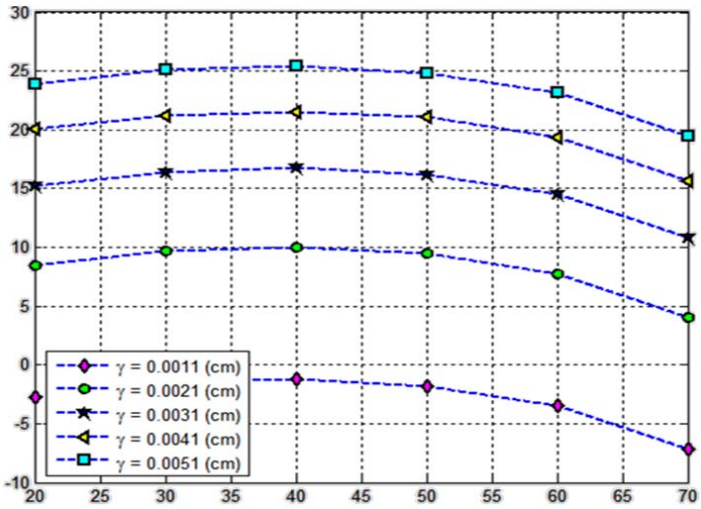

Fig. 38 $\boldsymbol{\sigma_{HH}}$ as a function of the incident angle $\boldsymbol{\theta}$ for different values of $\boldsymbol{\gamma}$

- *The impact of the multi-scale moisture parameter on the backscattering coefficient*

We can note in Figs. 39-41, that with an increase of the value of soil moisture, the amount of the backscattered signal will be higher and the depth of penetration of the radar signal will be lower. (x axe is the value of humidity %, and y axe is the backscattering coefficient dB).

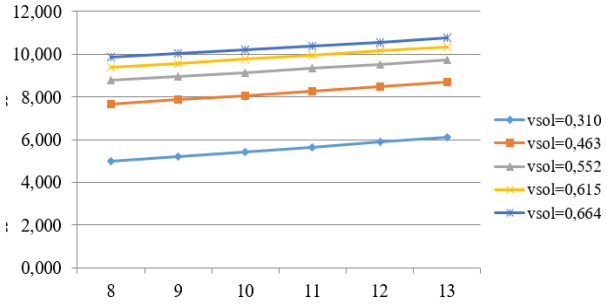

Fig. 39 $\boldsymbol{\sigma_{VV}}$ as a function of the incident angle $\boldsymbol{\theta}$ for different values of humidity

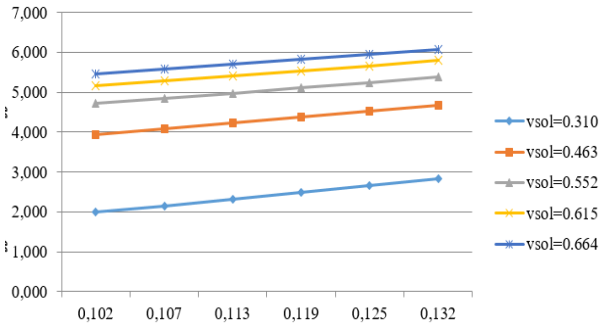

Fig. 40 $\boldsymbol{\sigma_{HH}}$ as a function of the incident angle $\boldsymbol{\theta}$ for different values of humidity

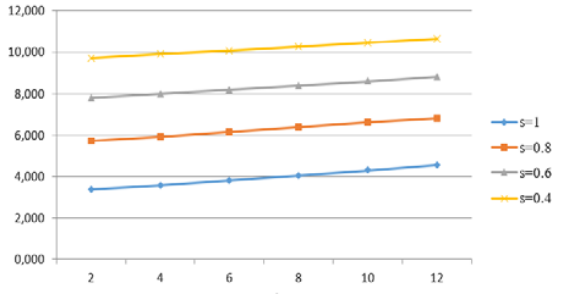

Fig. 41 $\boldsymbol{\sigma_{HH}}$as a function of the incident angle $\boldsymbol{\theta}$ for different values of $\boldsymbol{s}$

IV. Introduction of the Vegetal Layer on the Surface Soil Structure

A. Data from Remote Sensing

The vegetation occupies a large portion of the Earth's surface, and because of human agricultural activities, these natural resources have been allocated, particularly by the biodiversity, atmospheric composition and climate. Monitoring these areas has therefore become a very demanding environmental issue to treat.

The amount of vegetation or its density is an important geophysical parameter for many agronomic models, but also hydrological, meteorological or climate. In hydrology for example, vegetation plays the interception rainfall role, modifies the energy balance and water by transpiration, and finally it has a direct action on the filling level of the root layer of soil. In climatology, vegetation alters the aerodynamic roughness, which is an essential parameter of erosion processes [18].

Satellite remote sensing affords a valuable tool to provide geophysical information on a regional or global scale using microwave and optical sensors.

Optical sensors require illumination of the sun and clear sky conditions for measurements. In addition, optical data provide little information of the earth.

Contrariwise, the microwave remote sensing is able to obtain soil measurements regardless of weather conditions and at what time of the day, and thus it improves optical data.

There are two types of these sensors: active and passive sensors [19], [20]. Radiometers, passive sensors, measure the noise temperature from the thermal radiation of the observed scene. Furthermore, the radar, active sensors, measure the signal broadcast by the target.

The major drawback of the radar system is its low spatial resolution; this can be overcome by the use of SAR sensors (Synthetic Aperture Radar).

The SAR system is a technology that takes advantage of the satellite or aircraft movement where the radar system was installed in order to obtain the effect of an antenna aperture having a size larger than the real physical dimensions of the antenna, and finally acquire images with high resolution [19], [21], [22].

B. Comparison between the Active and Passive Remote Sensing for Estimating Soil Moisture

Getting information about the moisture content of the surface is important to assess the availability of soil water for plant growth in alpine meadows, and this can affect the duration of the grazing season, the rate of growth of grass and nutrient absorption.

Unfortunately, the spatial and temporal variations of soil moisture cannot be easily observed on a large scale using conventional measurement techniques. Radar Remote Sensing is an effective tool for the evaluation of soil moisture due to its dielectric constant witch is one of the most important factors influencing the radar backscatter intensity.

Active microwave systems offer the advantage of high resolution, but this comes at the expense of higher data rates and more complex treatment, while passive microwave systems offer the advantages of a frequent cover, low flow rates and a simpler data processing.

C. Synergistic Methodology Coupling of Optical and SAR Data for Estimating Physical Parameters of a Vegetation Zone

Several models simulating soil moisture from synthetic aperture radar data (SAR) have been developed for bare soil [7]-[11]. However, these models cannot be directly applied on vegetated areas; topsoil complicates the recovery of moisture in the basement-vegetation as it contains specific humidity [23]. Thus, the SAR acquisition corresponds to the combined signatures of water from vegetation water and soil water [15].

Because of the multiple scattering effects from the soil, the interaction between, the contributions of soil moisture and vegetation moisture on the one hand, and secondly of the observed backscattering radar signal, are highly non-linear. Therefore, the key problem in the quantitative estimation of soil moisture is to separate the contributions of the water content on vegetation and vegetated soil in radar backscatter.

The effects of vegetation on the SAR signatures are controlled by its biophysical parameters (e.g., vegetation cover and leaf area index), which may be obtained from optical remote sensing.

To minimize the effect of vegetation, some [16] attempted to use the additional plant information provided by optical remote sensing, which has been widely used to obtain information of vegetation biophysical properties. Moreover, other studies [16] suggested that the accuracy of soil moisture estimates were significantly improved when the optical and SAR data were combined compared with the estimates obtained based solely on SAR data.

The information on vegetation was extracted from optical remote sensing to correct SAR observations of vegetation based on a cloud model (WCM: Water Cloud Model [24]).

Radar backscatter is sensitive to roughness and soil moisture; however, in a vegetated area, it can also be affected by vegetation cover and the water content of plants. Therefore, the backscattering of a green area consists of the volume scattering vegetation and surface diffusion of the basement-vegetation attenuated by the vegetation layer.

The method is based on a synergistic microwave/optical model to simulate the radar backscatter from a green surface based on WCM model [24] and the two-dimensional SPM model. This SPM model was used to simulate the diffusion from a bare soil surface, and the WCM model was used to calculate the distribution of the volume and the bidirectional attenuation of vegetation.

1) Backscatter Bare Soil

The backscatter of bare soil surface mainly depends on the moisture content and the soil surface roughness. The multilayer two-dimensional SPM model is used to determine the backscatter of the basement-vegetation. In general, this model quantizes the backscattering coefficient of a surface roughness in terms of its parameters, its dielectric constant and the properties of acquired images (polarization, incident angle and frequency). Surface roughness is characterized by the RMS height and the correlation length. The dielectric constant is derived from the volumetric water content of the soil(σ_{sol}^0).

2) Vegetation Backscattering Model

The model was originally developed to describe the diffusion from only bare soil surfaces; Therefore, vegetation backscattering effects are not explicitly incorporated into the model [23]. WCM [24] is a mathematical model that was used to reduce the effect of vegetation, it considers the canopy like a cloud of water droplets that were randomly distributed. It has been used to determine the contribution of the vegetation using the leaf area index (LAI), the water content of the vegetation and biomass as canopy descriptors [11]. It was introduced by Attema and Ulaby [24] and was developed to predict the backscattering of a vegetated area.

In the WCM model, the total backscatter σ^0 is represented by the incoherent sum of the contribution of vegetation cover backscattering $\sigma_{veg}^0$and the contribution of the basement-vegetationσ_{sol}^0, mitigated by the vegetation layer and the interaction between the vegetated canopy and soil that is represented by multiple internal backscatter $\sigma_{veg+soil}^0$. Thus, the WCM can be represented for an incident angle θ by the following equation:

$$\sigma^0 = \sigma_{veg}^0(\theta) + \gamma^2(\theta)\sigma_{sol}^0(\theta) + \sigma_{veg+sol}^0 \quad (38)$$

$\gamma^2(\theta)$is the bidirectional attenuation coefficient of vegetation. Many modifications of WCM model have been reported [7], [20], [24].

We can conclude that for a given radar configuration, the backscatter of bare soil is a linear function of soil moisture. In addition, internal multiple interactions are not a dominant factor in the expression of the backscattering coefficient and can therefore be overlooked [25], [26]. Hence the modified equation is:

$$\sigma^0 = \sigma_{veg}^0(\theta) + \gamma^2(\theta)\sigma_{sol}^0(\theta) \quad (39)$$

$$\sigma_{veg}^0(\theta) = AV_1\cos(\theta)[1-\gamma^2(\theta)] \quad (40)$$

$$\gamma^2(\theta) = exp[-2\,V_2\,/\cos(\theta)] \quad (41)$$

V_1 and V_2 are respectively two topsoil descriptors, they describe the geometry effect of the cover canopy and the water content on the backscattering coefficient [24], [20], [26], [27]. A and$B$ are two empirical coefficients depending on the layer type.

The multilayered SPM model is used to replace the term of $\sigma_{sol}^0(\theta)$ in WCM model, and this replacement allows more realistic description of the bare soil moisture contribution in backscattering coefficient [14].

D. Sensitive Analysis of the Backscattering Coefficient Behavior

1) Multiscale Roughness Parameters Impact on Backscattering Coefficient

- *Fractal dimension effect*

We studied the impact of fractal dimension ν on backscattered radar signal by setting γ, the parameter related to the standard deviation of heights, at 0.0031m with a number of spatial scales P equal to 5 (Figs. 42 and 43).

We can note that the backscattering coefficient decreases with incident angle. Furthermore, higher the parameter ν, the backscattering coefficient decreases. This can be explained by the fact that the surfaces become smoother, and the diffusion properties are dominated by the specular reflection.

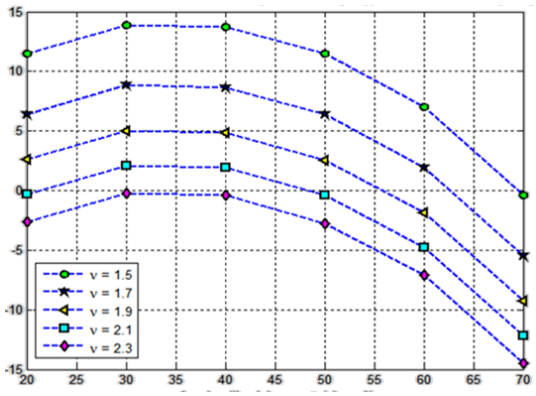

Fig. 42 $\boldsymbol{\sigma_{VV}}$ as a function of incident angle $\boldsymbol{\theta}$ for different values of $\boldsymbol{\nu}$

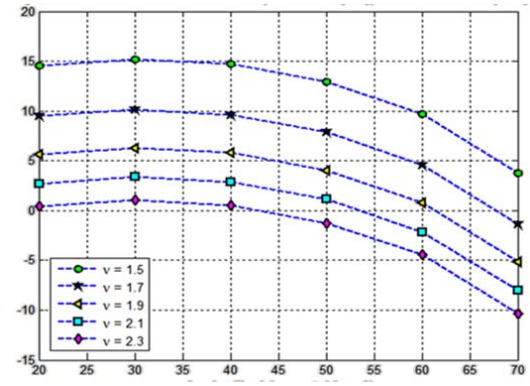

Fig. 43 $\boldsymbol{\sigma_{HH}}$ as a function of the incident angle $\boldsymbol{\theta}$ for different values of ν

- *The Effect of the Correlation Length*

ν was fixed to 1.3, and γ was varied from 0.0011m to 0.0051 m. In both cases, we note that the backscattering coefficient increases with γ.

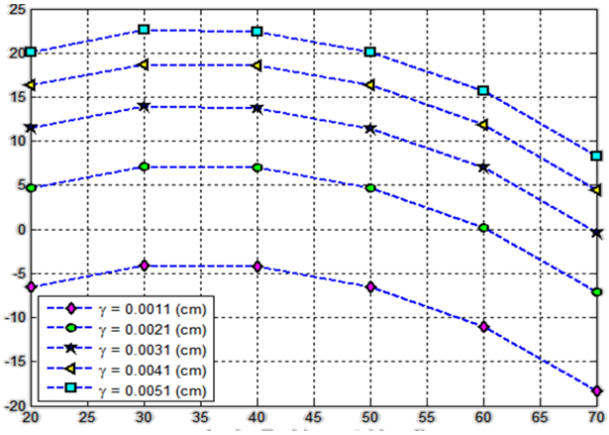

Fig. 44 $\boldsymbol{\sigma_{VV}}$ as a function of the incident angle $\boldsymbol{\theta}$ for different values of $\boldsymbol{\gamma}$

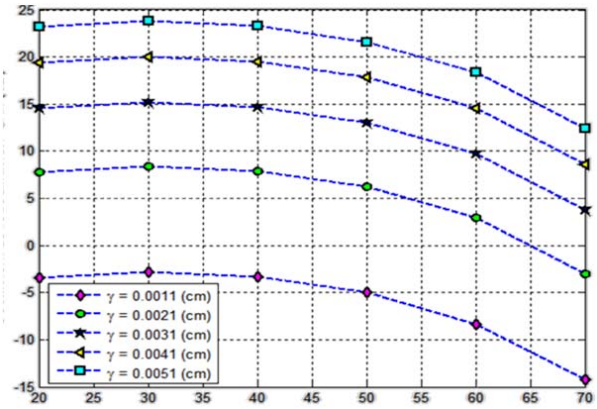

Fig. 45 $\boldsymbol{\sigma_{HH}}$ as a function of the incident angle $\boldsymbol{\theta}$ for different values of $\boldsymbol{\gamma}$

2) The Impact of Multi-Scale Moisture on Backscattering Coefficient

At first, the impact of ε' on radar signal backscattering by fixing ε" at 8 (Figs. 46 and 47) was studied and by varyingε' from 2 to 6 in both HH and VV polarizations. We notice that the backscattering coefficient increases as the complex dielectric constant ε' increases.

In Figs. 48 and 49, we set ε' at 5 and ranging ε" from 8 to 12. It is noted that when increasing ε", the backscattering coefficient increases as well. This is because when the soil gets wet, the amount of energy returned to the radar system decreases: the diffuse reflection is dominating in this case.

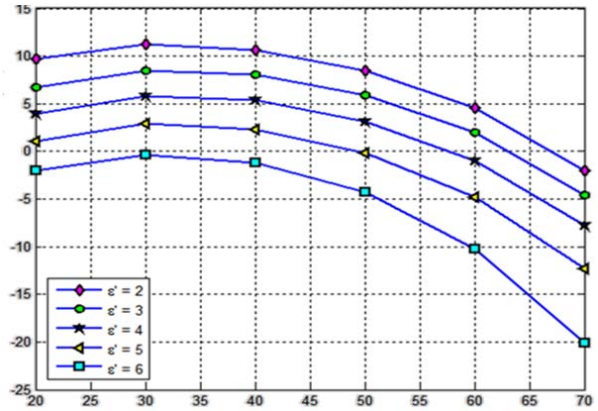

Fig. 46 $\boldsymbol{\sigma_{VV}}$ as a function of the incident angle $\boldsymbol{\theta}$ for different values of $\boldsymbol{\varepsilon'}$

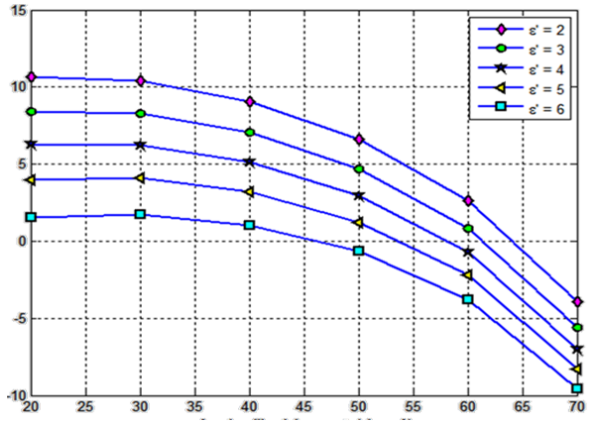

Fig. 47 $\boldsymbol{\sigma_{HH}}$as a function of the incident angle $\boldsymbol{\theta}$ for different values of $\boldsymbol{\varepsilon'}$

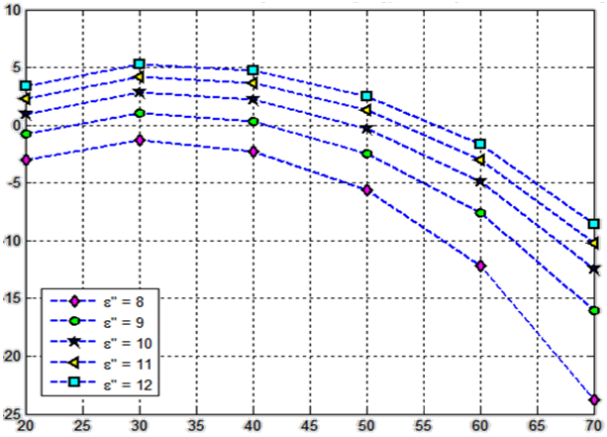

Fig. 48 $\boldsymbol{\sigma_{VV}}$ as a function of the incident angle $\boldsymbol{\theta}$ for different values of $\boldsymbol{\varepsilon}$"

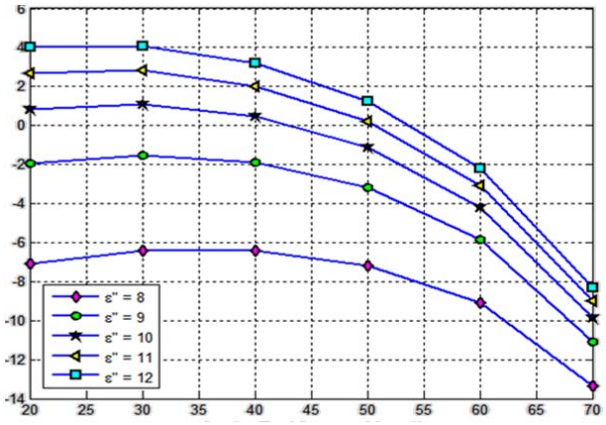

Fig. 49 σ_{HH} as a function of the incident angle θ for different values of ε''

V. Conclusion

The backscattering radar signal inversion in order to recover the physical parameters of large-scale natural surfaces is a major challenge for several applications in hydrology, geophysics and geology for predicting risks, monitoring the erosion and gully erosion. Data supplied by inversion process provide a comprehensive large-scale monitoring of natural surfaces over time and enabling firstly a major time savings compared to conventional data collection and secondly a broader vision.

References

[1] F, Adrian, L, Zongqian, and Kun-Shan, "Backscattering from a randomly rough dielectric surface", IEEE Transactions on Geoscience and remote sensing, vol. 30, no. 2, p. 356-369, 1992.

[2] O, Yisok, S, Kamal, and U, Fawwaz. "An empirical model and an inversion technique for radar scattering from bare soil surfaces". IEEE transactions on Geoscience and Remote Sensing, 1992, vol. 30, no 2, p. 370-381, 1992.

[3] M. Autret, R. Bernard, and D. Vidal-madjar. "Theoretical study of the sensitivity of the microwave backscattering coefficient to the soil surface parameters". Remote Sensing, vol. 10, no 1, p. 171-179, 1989.

[4] W.-K. Chen, *Linear Networks and Systems* (Book style). Belmont, CA: Wadsworth, 1993, pp. 123–135. J. Souyris, L. Wang, and C. Hsu. "Inversion of soil moisture with radar backscattering data". In: Geoscience and Remote Sensing Symposium, IGARSS'94. Surface and Atmospheric Remote Sensing: Technologies, Data Analysis and Interpretation., International. IEEE, p. 1392-1394, 1994.

[5] MD. Zribi, "Development of new methods for modeling the roughness and microwave backscatter from the ground surface". University Paul Sabatier Thesis, specialty signal processing and remote sensing, p. 1-181, 1998.

[6] L. Fung. "A study of the IEM further Top surface scattering model", IEEE Transactions on Geoscience and Remote Sensing. vol. 35. -p. 901-909, 1997.

[7] H, Martti T., Ulaby, T. Fawwaz and C. Myron. "Microwave dielectric behavior of wet soil-part 1: Empirical models and experimental observations". IEEE Transactions on Geoscience and Remote Sensing, no 1, p. 25-34, 1985.

[8] R. James, and J. Thomas. "An empirical model for the complex dielectric permittivity of soils as a function of water content". IEEE Transactions on Geoscience and Remote Sensing, no 4, p. 288-295, 1980.

[9] B. Bouman. "Crop parameter estimation from ground-based X-band (3-cm wave) radar backscattering data". Remote Sensing of Environment, vol. 37, no 3, p. 193-205, 1991.

[10] P. A. Burrough, "Fractal dimensions of landscapes and other environmental data." Nature, vol. 294, no 5838, p. 240, 1981.

[11] F. Mattan, and T. Le Toan. "Backscattering properties of multi-scale rough surfaces". Journal of Electromagnetic Waves and Applications, vol. 13, no 4, p. 493-527, 1999.

[12] L. B. Farah, I. R. Farah, and R. Bennaceur. "Soil multi-scale roughness parameters and soil moisture retrieval from radar backscattering using a neural network technique". In: PIERS Proceedings. p. 2-5, 2006.

[13] M. Zribi, Mehrez, A. Lemorvan, and N. Baghdadi. "Dielectric constant modelling with soil–air composition and its effect on SAR radar signal backscattered over soil surface". Sensors, 2 vol. 8, no 11, p. 6810-6824, 2008.

[14] S, Kaijun, Z, Xiaobing, and F, Yong. "Multilayer soil model for improvement of soil moisture estimation using the small perturbation method." Journal of Applied Remote Sensing, vol. 3, no 1, p. 033567, 2009.

[15] D, Malcolm, J. le Toan, and M, Francesco." On the characterization of agricultural soil roughness for radar remote sensing studies". *IEEE Transactions on Geoscience and Remote Sensing*, vol. 38, no 2, p. 630-640, 2000.

[16] L. Farah. "A Two Layers Multiscale Bi-dimensional SPM Model for Study of Radar Backscatter Behavior is Semi-arid Soil subsurface", Piers Online (Progress In Electromagnetic Research). - 2010.

[17] S. Mallat, "A theory for multiresolution signal decomposition: the wavelet representation". IEEE transactions on pattern analysis and machine intelligence, vol. 11, no 7, p. 674-693, 1989.

[18] B. Marticorena, B, Gilles, and G. Dale. "Factors controlling threshold friction velocity in semiarid and arid areas of the United States." Journal of Geophysical Research: Atmospheres, vol. 102, no D19, p. 23277-23287, 1997.

[19] U, Fawwaz,, M. Richard, and F. Adrian. "Microwave remote sensing: Active and passive, volume ii: Radar remote sensing and surface scattering and emission theory". Artech house, p. 855, 1982.

[20] F. Ulaby, and T. Allen." Relating the microwave backscattering coefficient to leaf area index". Remote Sensing of Environment, vol. 14, no 1-3, p. 113-133, 1984.

[21] C; Elachi. "Introduction to the Physics and Technology of Remote Sensing". 1987.

[22] J. R McDonough. SyntheticApertureRadar: Systems and Signal Processing. 1991.

[23] L. Tsang, A. Kong and J. Shin. "Theory of Micro-Wave Remote Sensing". John Wiley, Hoboken, NJ - 1985.

[24] E. Attema, and F. Ulaby. "Vegetation modeled as a water cloud." Radio science, vol. 13, no 2, p. 357-364, 1978.

[25] M. dobson, and F. Ulaby. "Active microwave soil moisture research". IEEE Transactions on Geoscience and Remote Sensing, no 1, p. 23-36, 1986.

[26] L. Prevot., I. Champion, G. Guyot, "Estimating surface soil moisture and leaf area index of a wheat canopy using a dual-frequency (C and X bands) scatterometer". *Remote Sensing of Environment*, vol. 46, no 3, p. 331-339, 1993.

[27] H. Mcnain, B. Brisco. "The application of C-band polarimetric SAR for agriculture: a review." Canadian Journal of Remote Sensing, vol. 30, no 3, p. 525-542, 2004.